An EUV Fresnel zoneplate mask-imaging microscope for lithography generations reaching 8 nm

Kenneth A. Goldberg[*a], Iacopo Mochi[a], Senajith B. Rekawa[a], Nathan S. Smith[a], James B. Macdougall[a,b], Patrick P. Naulleau[a]

[a]Center for X-Ray Optics, Lawrence Berkeley National Laboratory, Berkeley, CA 94720
[b]Department of Physics, California State University, Fresno, CA 93740

ABSTRACT

We present the potential optical performance capabilities of a next-generation extreme ultraviolet (EUV) mask-imaging microscope, based on the proven optical principle of the SEMATECH Berkeley Actinic Inspection Tool (AIT), but surpassing it in every performance metric. The new synchrotron-based tool, referred to here as the SEMATECH Berkeley Actinic Imaging Tool at 0.5 NA (AIT5) will enable research on multiple generations of EUV lithograpy design rules. The proposed microscope features an array of user-selectable Fresnel zoneplate lenses with diffraction-limited quality and different optical properties, such as numerical aperture (NA) and magnification. An efficient all-EUV optical system with variable high magnification and direct EUV detection provides images with the highest possible signal-to-noise ratio. A lossless, customizable-coherence illuminator based on angle-scanning mirrors and an ellipsoidal condenser creates arbitrary pupil fill patterns, with partial coherence σ values up to 1.0 at 0.5 4×NA and higher. In combination with rotated zoneplate objective lenses, the illuminator will be capable of a range of discreet aziumuthal angles as well, modeling the behavior of EUV steppers across a ring-field of view.

Keywords: extreme ultraviolet lithography, EUV, microscope, actinic, mask, reticle, imaging, zoneplate

1. INTRODUCTION

Owing to the wavelength-specific reflective properties of EUV reticles, imaging with EUV light is the only faithful way to understand the physical response of defects, repairs, and pattern bias and optical proximity corrections. These properties limit the effectiveness of all non-EUV inspection technologies, and it is likely that the differences between EUV and non-EUV measurement technologies will increase in future nodes. Therefore, the prolonged unavailability of a high-quality, high-resolution, EUV "actinic" mask-imaging microscope tool could hamstring the commercialization of EUV lithography, and impede research into future nodes.

Despite this pressing need,[1,2] the availability of commercial tools is still several years away.[3,4] Prototypes and research tools have been at the forefront of actinic mask research for over a decade,[5] and they may continue to chart the course, reaching forward to explore future nodes and ever-higher resolutions.

We have operated the SEMATECH Berkeley Actinic Inspection Tool (AIT) at Lawrence Berkeley National Laboratory since 2004, an industry-funded research project dedicated to EUV photomasks. As a high-magnification, all-EUV, Fresnel zoneplate microscope, the AIT has been in the vanguard of high-resolution EUV mask imaging for several years. The AIT's measurement of mask architectures, blank and pattern defect imaging,[6,7] defect smoothing and printability,[8,9] multilayer phase roughness,[10] and recently, direct, quantitative aerial image phase measurement,[11] has expanded our collective understanding of EUV masks and shaped the course of current mask development. Yet the AIT is reaching its seventh year of operation, and its inflexible design will prevent it from participating in the numerous necessary advances that are part of the ongoing race to commercialize EUV lithography.

[*] KAGoldberg@lbl.gov; phone 1 510 495-2261; fax 1 510 486-4550; goldberg.lbl.gov

1.1 Need for a new tool

Despite its success and continued usefulness, the AIT faces significant optical and mechanical shortcomings for the continued evolution of EUVL toward future technology generations with design rules at and below 16-nm. To achieve its current level of performance, significant efforts have been made to retrofit the AIT and adapt to its original design limitations.[12,13,14] A new tool could greatly surpass the capabilities of the AIT by overcoming many of its shortcomings. The AIT lacks kinematic mask positioning, and with its rotation-translation stage (originally designed for rotational scanning[15]) and absence of an *in situ* visible-light microscope, mask navigation can be slow and challenging. In some cases the AIT loses positioning accurcy for mm-scale moves; for this reason, defects and pattern features of interest must be easily identifyiable, or marked in a clear way to avoid tedius and time-consuming searches. Mechanical instability makes the AIT sensitive to vibration from environmental sources. To achieve stable imaging, the zonepalte stage gently touches the mask surface at one point during exposure. During navigation, the two stages are decoupled, resulting in vibration-induced micron-scale image blur that makes it challenging to identify fine features, including defects.

Beyond the mechanical and navigation difficulties, progress with the AIT is also limited by its optical design. A 20× Schwarzschild objective serves as the condenser optic focusing light onto the mask with a fixed, 6° angle of incidence.[12] The Schwarzschild occupies a large space above the mask and zoneplate lens, forcing the use of a small, difficult-to-align turning mirror to direct the beam horizontally toward the charge-coupled device (CCD) detector. The elimination of this mirror in a future design would improve efficiency and simplify the alignment. While the Schwarzschild has a relatively large solid angle—about 0.1 numerical aperture (NA) in an unobstructed subaperture—it delivers relatively high-coherence illumination that we have estimated to be close to σ of 0.2.[12] This unusual situation arises from the low divergence angle (and relatively high coherence) of the input beam that the Schwarzschild objective demagnifies. The most significant drawback of the Schwarzschild is that it has become highly contaminated over time and cannot be accessed for cleaning, rotation, or replacement without dismantling the system. Based on the relatively high intensity of the beam at the edges of the condenser's pupil, which we observe by intentionally mis-aligning the beam, we estimate that the efficiency of the Schwarzschild is below 20% of its original value in the center of the pupil.

In summary, there are a number of issues that can be corrected with a more advanced optical design, leading to the creation of a more efficient system with simplified alignment, an adjustable angle of incidence to accommodate future EUV generations with higher NA values, and a fully customizable illuminator to emulate the aerial image produced by current and future lithography tools.

A working name for new microscope is "The SEMATECH Berkeley Actinic Imaging Tool at 0.5 NA" or "AIT5." This name was chosen for synergy with a parallel project in our group, "The SEMATECH Berkeley Micro-field Exposure tool at 0.5-NA" or "MET5."

2. SIGNIFICANT ASPECTS OF THE DESIGN

The AIT5 design preserves the most successful aspect of the AIT (zoneplate imaging) while replacing and updating all of the design elements responsible for its shortcomings. The new concept borrows heavily from proven designs used in other, successful EUV and soft x-ray experimental tools including The SEMATECH Berkeley MET[16] and XM-1.[17] The greatest improvements will be realized in the areas of (1) resolution, (2) coherence control, (3) mask and zoneplate stages, (4) flux reaching the detector, (5) vibration isolation and stability, (6) maintenance and alignment, and (7) ease of use. Significant aspects of the design are briefly described here, with additional information on the illuminator and high-magnification imaging system, provided in Sections 3 and 4. This paper focuses on the optical design, illumination and resolution considerations. Predicting specific imaging performance metrics beyond resolution is the subject of ongoing research.

The project's goal is to create an operationally flexible system that minimizes the number of mirrors and moving parts, and maximizes quantitative feedback on beam position, size, and power. Where possible, the design incorporates flat mirrors that can be adjusted or easily replaced. An open design framework will enable access for routine system maintenance, while internal baffles and a minimum number of moving parts will protect the mask from particles.

Figure 1 shows a schematic of the beam path through the optical elements of the beamline and endstation. Its salient features are described in the following sections.

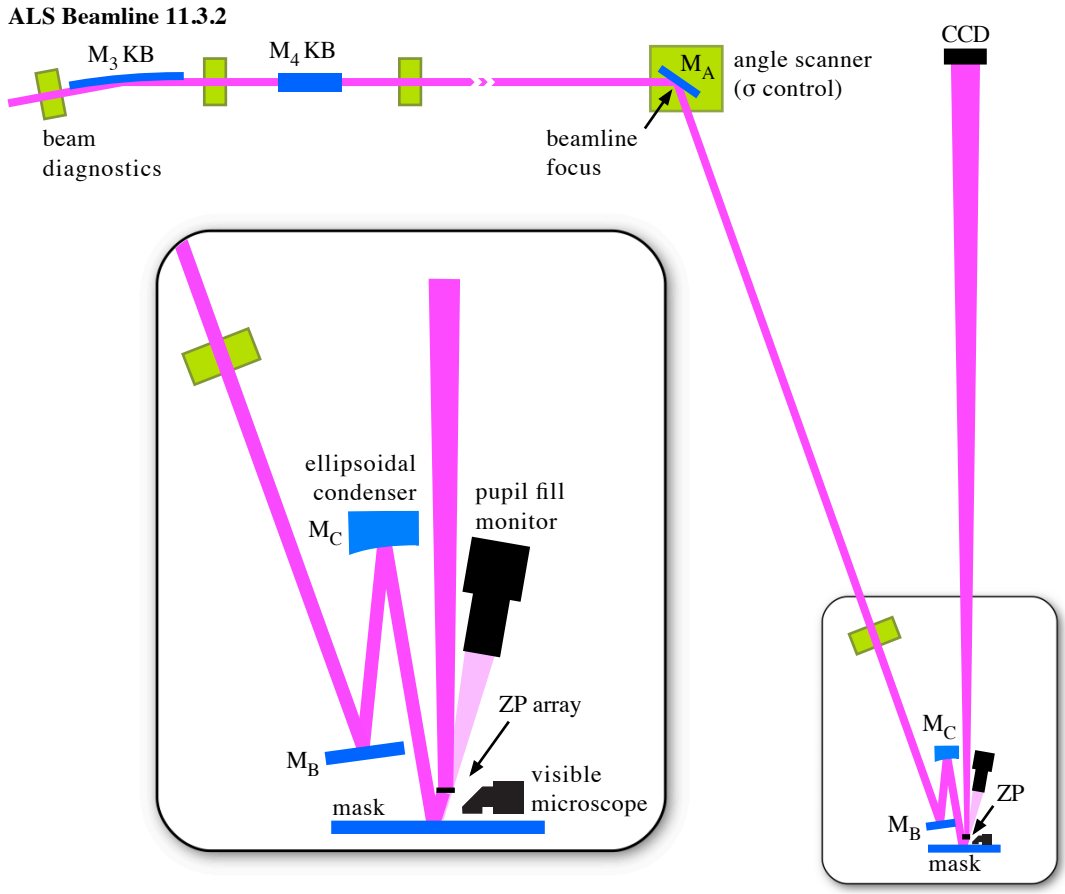

Figure 1. A schematic layout of the AIT5 beamline illuminator and imaging system. The Fourier-synthesis illuminator consists of KB mirrors with an intermediate focus on angle-scanning mirror M_A, a flat turning mirror M_B (inset), and an ellipsoidal condenser mirror M_C to illuminate a small region of the mask. The imaging system consists of a single zoneplate lens (from an array) that projects a high-magnification aerial image (M ~ 1000) onto a EUV-sensitive CCD camera. A pupil-fill monitor examines the angular properties of the illuminating beam directly by recording the zero-order light, before or during exposure. A visible-light microscope positioned within a few cm of the zoneplates aids mask navigation. Various beam position monitors analyze the beam location (and angle), size and power at important locations for mirror alignment.

2.1 Beamline efficiency, focusing and alignment control

The AIT5 will use the same beamline source that now powers the AIT, with modifications that deliver greater efficiency and an optimized divergence angle, and with new alignment diagnostics for beam focusing and position feedback. A pair of elliptically bent mirrors (Kirkpatrick-Baez, configuration) provides two-dimensional focusing onto the first mirror of the illuminator, M_A. Our goal is to produce a 150×150-μm spot (or smaller) with divergence angles below 5 mrad. The beamline now produces approximately 13.4 μW of EUV light within a narrow bandwidth ($\lambda/\Delta\lambda \sim 1500$) at the M_A position. We are investigating the efficiency gains that may be achievable using a new monochromator grating, produced with an HSQ surface smoothing technique[18] that has been demonstrated in other EUV and soft x-ray beamlines. Since beam alignment and position monitoring are critical to aberration minimization, repeatable illumination conditions, and tool uptime, we will create a series of compact beam position monitors with fiducial features that can be registered to absolute positions outside of the vacuum chamber. Beam position, angle, and flux levels will be assessed repeatedly, as necessary to maintain performance.

2.2 Mask and zoneplate stages

Stable imaging requires that the mask and zoneplate objective lens remain stationary with respect to each other on a nm length scale during the exposure. To provide stability, the AIT5 will have a shared internal frame that supports the mask and zoneplate stages together, held by an active and passive vibration-isolation system. An *xyz* mask stage will provide enough travel to enable measurements across the entire mask surface. A second *xyz* stage supports the array of zoneplate lenses. The other optical elements, and components in the system do not have the same stability requirements as the mask and zoneplate stages, and they will be supported separately.

2.3 Improved navigation with *in situ* microscopes

The AIT5 will have several tools to facilitate rapid navigation across the mask pattern. First, an *in situ* visible-light microscope, within a few cm of the zoneplate lenses, will provide a low-magnification view of a 1 to 2-mm-wide area of the mask. The mask stages will allow the microscope to image the entire mask surface. Second, the AIT5 will have at least one low-magnification zoneplate lens that will provide a wider view of the mask surface. The zoneplate stage will enable switching between zoneplate lenses in seconds—comparable to the way a standard laboratory microscope operates with interchangeable lenses. Finally, an additional navigational aid is an external mask "photo box" that records a photographic image of the mask surface, and imports that image into the AIT5's navigation software to guide the operator. This photograph serves as a map of the whole-mask surface, revealing the positions of large, identifiable features, or the spacing between patterns on the mask, when that information has not been provided to the operator.

2.4 Environment

The vacuum chamber will be created following UHV standards, using EUVL-appropriate materials that enable base pressures in the mid-10^{-7} Torr range, with final assembly performed in a clean room. The tool itself will be housed in a cleanroom enclosure that provides acoustic noise damping inside the ALS experiment hall. The cleanroom specifications have not yet been determined.

3. ILLUMINATOR

The AIT5 illuminator will enable lossless, customizable pupil-fill patterns, based on the *Fourier-synthesis illuminator* concept implemented by Naulleau[19,20] for synchrotron beamlines and coherent sources. The illuminator uses the relatively narrow divergence angle and intrinsically high coherence of the beamline, in combination with scanning mirrors, to rapidly fill the angle-space in time, during each exposure.

3.1 Three-mirror illuminator concept

The AIT5 illuminator consists of three multilayer-coated mirrors—two flat and one diamond-turned ellipsoid—to illuminate a small spot on the upward-facing surface of the mask. A schematic layout is shown in Fig. 2. We label the mirrors M_A, M_B, and M_C, in order. The beamline focuses EUV light to a stationary, 150-μm-diameter spot on M_A. This spot is demagnified 10:1 by the ellipsoidal M_C condenser forming a 15×15-μm mask-illumination area with relatively high spatial coherence ($\sigma \leq 0.2$). With programmable angle scanning from M_A during exposures, the system "paints out" arbitrary pupil fills in time.

3.1.1 Angle-scanning mirror M_A. Mirror M_A is flat turning mirror with an angle of incidence greater than 45° from normal. The stationary beam footprint on the mirror acts as a virtual source point for the illuminator. M_A will be able to move out of the beam path, to enable beamline-focusing diagnostics to probe the size and position of the beam at the intermediate focus.

M_A creates the angular fill patterns by scanning angle in time. The 10:1 demagnification enables small M_A angle changes to become large angle changes at the mask. Filling a 0.5 4×NA pupil with partial coherence σ of 1.0, for example, requires an angular range of ±7.2° at the mask, and thus only 0.72° (12.6 mrad) from the angle scanner. The required mirror tilt range is half of this value. The scanning frequency (up to ~500 Hz) will be high enough to enable the mirror to scan the same pattern several times within the exposure time.

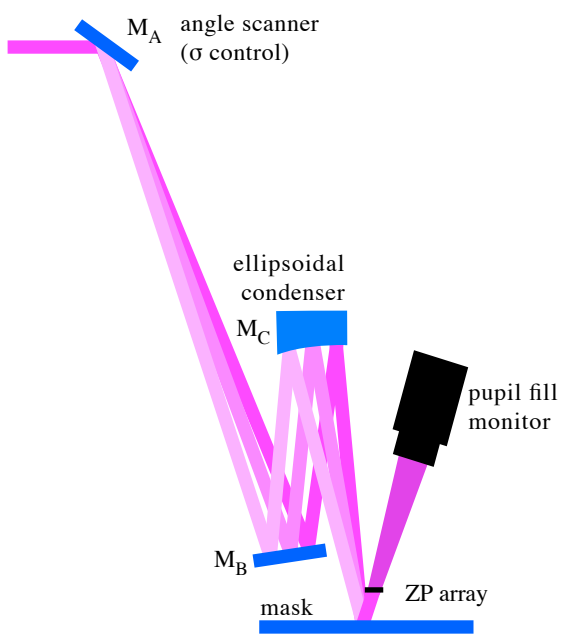

Figure 2. A schematic of the AIT5 Fourier-synthesis illuminator (not to scale). The beamline's intermediate focal point on M_A is re-imaged onto the mask with 10× demagnification by the M_C ellipsoidal condenser mirror. As the angle of M_A is adjusted, the beam footprint on the mask remains stationary. Illumination uniformity can be improved by performing small oscillations (μrad) of the M_C angle during exposure. The zoneplate's first diffraction order projects the image of the mask upward (not shown).

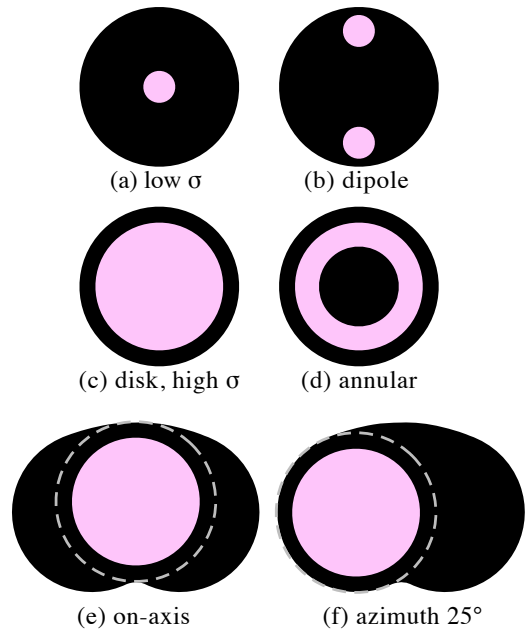

Figure 3. **(a–d)** Examples of pupil-fill patterns achievable with the Fourier-synthesis illuminator. **(a)** The highest coherence state will be achieved with the M_A mirror remaining stationary (and possibly restricting the divergence with an aperture). The condenser is designed to provide high σ values (0.8–1.0) for 4×NA values up to 0.625. Smaller NAs will simply use a smaller fraction of the condenser's angular range. **(e–f)** Azimuthal rotation of the central ray axis (to emulate cross-smile behavior in an arc-shaped field) can also be achieved simply by steering the central angle to one side or the other.

3.1.2 Turning mirror M_B. The illuminator geometry requires a folding mirror close to the mask surface to reflect the incident light upward into the condenser, M_C. Mirror M_B keeps the central incidence angle and the range of angles across the condenser low, simplifying the ellipsoid's multilayer coating design.

3.1.3 Condenser M_C and the controllable pupil-fill patterns. The ellipsoidal condenser is the only element with power in the illuminator. Mirror M_C reduces the 150-μm spot on M_A to a 15-μm spot on the mask. Since each ray leaving the beam spot on M_A is refocused by the condenser to a single point on the mask, we can accommodate different illumination angles, partial coherence fill patterns and azimuthal angles by steering the central ray and angular pattern using M_A. By design, M_C is large enough to accommodate a wide range of input conditions.

The central angle of incidence on the mask can be adjusted from 6° up to 10° with a small adjustment of M_A (0.2°) and no change to M_C. Without scanning, the beam footprint on M_C is expected to be a few mm wide. This beam size (and the zoneplate NA) determines the smallest achievable partial-coherence σ value in the system. We estimate that the minimum σ value could be as low as 0.2 for a 0.25 4×NA lens, and approximately 0.1 when a higher 4×NA objective (0.5 or greater) is used.

Creating a high-quality M_C mirror will be a challenge, though the figure specifications are several orders of magnitude less strict than EUV projection optics. For the mask, the stationary beam footprint goal is 15-μm diameter. To control the beam position to within 5 μm, the M_C figure must have slope errors of 25 μrad or smaller, including misalignment errors. Building on the work of scientists at Lawrence Livermore National Laboratory[21], members of our group have demonstrated that multilayer-coated diamond-turned optics can be made considerably smoother through the application of HSQ before coating,[22] reducing the amplitude of the characteristic groove pattern of the diamond turning fabrication process.

Figure 3 shows a representation of various pupil-fill patterns that will be possible with the illuminator. To achieve appropriate sigma values for different NA and incidence angle, smaller or larger portions of the M_C mirror can be used.

3.1.4 Spanning the azimuthal angles of incidence. The illuminator design also enables the AIT5 to provide arbitrary azimuthal angles of incidence, to model imaging behavior across the *smile* of an EUV stepper. In other words, the plane of incidence can be rotated away from the usual straight-ahead plane by steering the M_A central scanning angle. We are now investigating the maximum range of azimuthal angles required to emulate current and future steppers and its impact on the multilayer coating requirements of M_C. The beam footprints for two azimuthal angles are shown in Fig. 3e and f.

3.1.5 Pupil-fill monitor. To achieve reliable and consistent angular fill patterns, the illuminator requires a pupil-fill monitor to provide direct visual feedback that is not available from the image alone. Our concept is to place a removable, EUV to visible-light microscope to capture the beam reflected from the mask. Using an empty aperture in place of the zoneplate, we can observe the illumination pattern relative to the pupil's cutoff angles. Provided there is sufficient light, a second technique is to record the zero-order beam during the imaging of a bright mask region, as shown in Fig. 2.

3.2 Field uniformity scanner

To achieve a high level of illumination uniformity, or to increase the size of the illuminated area when required, it will be necessary to scan the focused beam across the field of view using a two-dimensional pattern, uncorrelated from the timing and pattern of the angle-scanner. We can achieve this effect without disrupting the partial-coherence control by scanning either M_B or M_C through very small angular deviations. Displacing the beam spot on the mask by 15 μm, for example, requires M_B or M_C angle changes of approximately 50–80 μrad (0.003°). With this scanning, there may be a necessary trade-off between uniformity and flux density (and thus exposure time).

4. IMAGING SYSTEM DESIGN AND PERFORMANCE

The AIT5's zoneplate objective lenses are similar to those in the current AIT. Individually, they are single, off-axis Fresnel zoneplate lenses that project the image with high magnification and diffraction-limited quality[23] onto an EUV-direct-detection CCD camera. An array of interchangeable zoneplate lenses on the same substrate allows us to adjust the imaging parameters discussed here.

The nominal distance from the zoneplate to the mask is 750 μm in the AIT, and the magnification ratio is typically 907. The AIT5 will increase the magnification ratio to 1000 by a combination of shortening this focal length and by increasing the distance to the CCD. If a similar CCD camera model is used, with a 2048×2048 array of 13.5 μm square pixels, the effective pixel size will be 13.5 nm in mask units. While this magnification provides an acceptable pixel oversampling for several generations of higher resolution EUV masks, it can be increased in the future, by extending the distance to the CCD. There is an important trade-off between magnification and the signal to noise ratio for fixed exposure times—the light intensity falls as the square of the magnification.

The interrelated properties of lens diameter, NA, angle of incidence, bandwidth requirement, focal length, field of view, magnification ratio, and sweet spot diameter cannot be adjusted independently. Selecting the optimal zoneplate design requires making various tradeoffs; but since an array of different, interchangeable zoneplates can be installed, the optimal parameters for a given experiment can be selected. The AIT5 will have a stable, precise zoneplate stage capable of switching between zoneplates in seconds.

Figure 4 schematically shows the mask and zoneplate-array arrangement in the AIT and AIT5. The primary difference is the removal of a small folding mirror placed immediately above the zoneplates in the AIT, to direct the beam outward from under the Schwarzschild objective that sits above it. The fine-alignment and quality of this mirror has been a major concern for the AIT. The AIT5 projects the image, in the zoneplate's first diffracted order, upward onto the CCD camera, simplifying alignment, improving efficiency, and eliminating the potential for contamination and imperfections in the turning mirror to affect the imaging. Rather than send the beam in the directly vertical direction, a small tilt could be added to the zoneplate design to steer the image away from the closest edge of M_C.

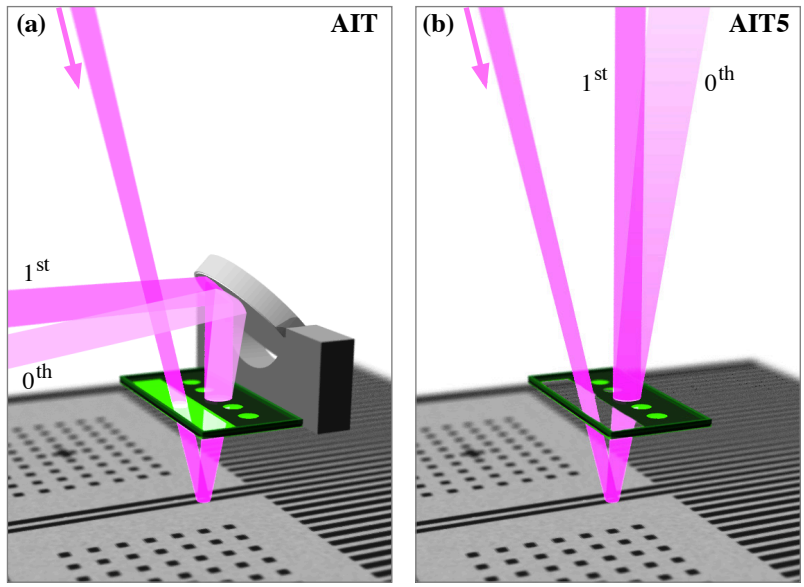

Figure 4. Schematic representation of the imaging systems in the **(a)** AIT and **(b)** AIT5, including the beam, mask, zoneplate array. The turning mirror in AIT was necessary to avoid the Schwarzschild objective, directly above the mask. Eliminating the turning mirror in AIT5 will greatly simplify alignment and improve efficiency. Improved nanofabrication techniques should also enable an increase in the zoneplate efficiency through the removal or thinning of the silicon nitride window for the incident beam.

4.1 Variable NA

The array of zoneplate lenses provides the opportunity for many different NA values, off-axis angles of incidence, azimuthal rotation angles (i.e. across the smile), and magnifications, as shown schematically in Fig. 5. Each zoneplate will be specified for one set of these four parameters. Our work with the AIT has demonstrated high-quality imaging with 6° incidence and 4×NA values up to 0.35. Higher off-axis angles of incidence enable increasingly large 4×NA values, which we predict can go up to 0.625 (0.156 mask-side NA) at 10° for circular pupils. To block the undiffracted zeroth-order zoneplate light from reaching the CCD and overlapping the first-order image, we impose a practical constraint on the maximum allowable circular zoneplate aperture. Rays from the mask surface should not come within a *buffer angle*, β, from vertical. The angle is chosen based on the CCD camera width and position, and will typically be 1°, or slightly smaller. Figure 6 shows the maximum 4×NA values for different angles of incidence, θ, and buffer angles.

The need to block the overlapping zeroth order light only applies in the section of the lens pupil closest to the vertical ray (the mask normal ray). In principle, lenses with considerably higher solid angle, in both lateral directions, could be created for ultra-high-resolution measurements—although those pupil shapes would not be rotationally symmetric, or centered on the central ray angle, so their imaging properties would not be representative of conventional steppers.

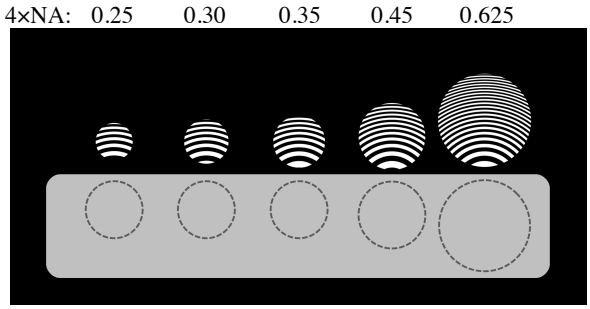

Figure 5. A schematic representation of an array of off-axis zoneplates with different NA and angle of incidence values. The light gray area is a window for the incident beam; black areas are opaque to EUV light. The dashed circles indicate the window region where the illuminating beam will pass through. The zoneplate pupils are centered on the central ray of the light reflected from the mask.

Figure 6. To prevent the undiffracted zeroth order zoneplate light form reaching the CCD camera and overlapping the image (causing loss of contrast), the zoneplate aperture must block rays close to vertical. We define a buffer angle β, based on the width and position of the CCD camera. We anticipate using a β value between 0.5 and 1°. The plot shows the maximum allowable NA value given different angles of incidence and buffer angles.

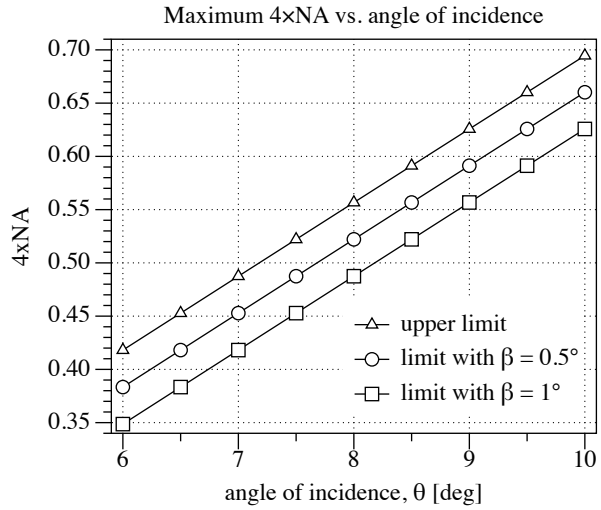

4.2 Resolution

Table 1 and Fig. 7 contain resolution-limit calculations for various NA and σ values in the AIT and the AIT5. Prolith[24] calculations for the AIT are consistent with observed performance: 46% contrast in 64-nm lines was measured using a 0.35 4×NA objective lens.[25] With σ = 1.0, the AIT5 should be able to achieve mask-scale dense-line imaging with 35-nm half-pitch (hp) at 50% contrast (equivalent to 8.75 nm, at the wafer).

Figure 8 shows the calculated contrast from dense line features for various 4×NA values from 0.25 to 0.625. At the highest NA shown, the contrast at 8-nm hp is close to 50%. With σ values above 0.8, the small-feature contrast could be further enhanced.

Table 1. Expected resolution limits for the AIT and AIT5 based on relevant NA and σ values.

			coherent resolution limit σ = 0.0 ½*1.22*λ/NA		**incoherent resolution limit σ = 1.0** ¼*1.22*λ/NA		**Prolith model** Dense Lines 50% Contrast		
	Mask NA	Wafer NA	Mask [nm]	Wafer [nm]	Mask [nm]	Wafer [nm]	system:	Mask [nm]	Wafer [nm]
	0.0625	0.250	130.8	32.7	65.4	16.3			
	0.0750	0.250	109.0	27.2	54.5	13.6			
AIT practical limit, 6°	**0.0875**	**0.350**	**93.4**	**23.4**	**46.7**	**11.7**	AIT σ = 0.2	70	17.5
	0.1000	0.400	81.7	20.4	40.9	10.2			
	0.1125	0.450	72.7	18.2	36.3	9.1			
AIT5 0.5-NA design	**0.1250**	**0.500**	**65.4**	**16.3**	**32.7**	**8.2**			
	0.1375	0.550	59.4	14.9	29.7	7.4			
	0.1500	0.600	54.5	13.6	27.2	6.8			
AIT5 max at 10°	0.1563	0.625	52.3	13.1	26.2	6.5	AIT5 σ = 1.0	35	8.75

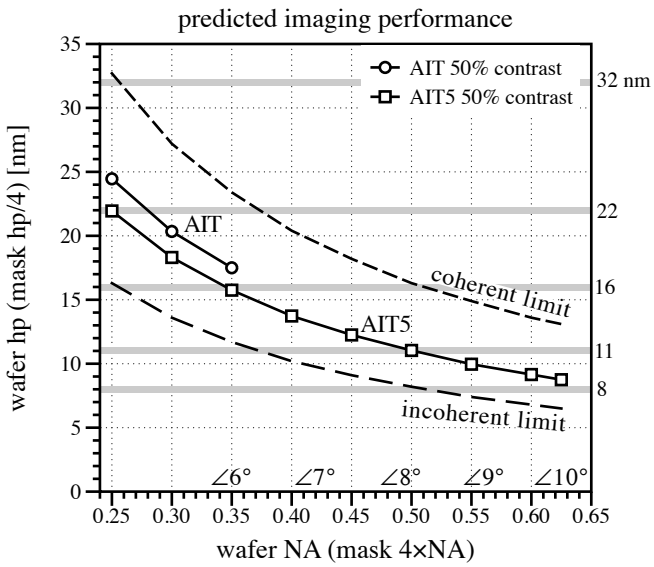

Figure 7. Calculated coherent and incoherent resolution limits of the AIT and AIT5 (dashed lines) as a function of NA. Solid lines show the resolution for a range of NA values at $\sigma = 0.2$ (AIT) and $\sigma = 0.7$ (AIT5). Operation at higher NA values requires larger angles of incidence to maintain a circular pupil shape that does not overlap the vertical ray.

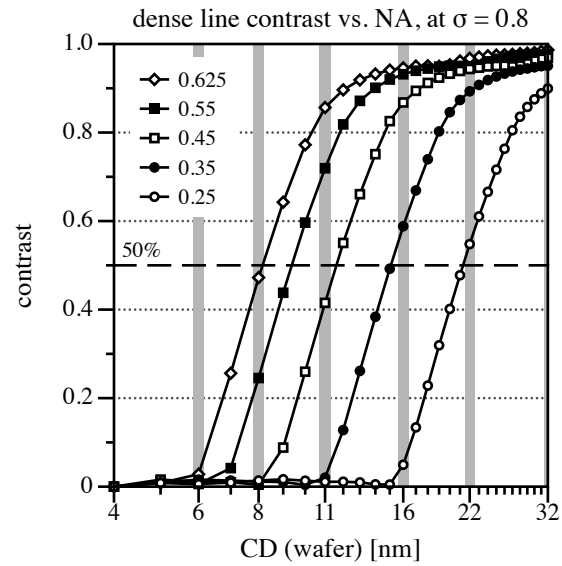

Figure 8. Calculated AIT5 dense line image contrast for a range of 4xNA values between 0.25 and 0.625 with circular pupils. Higher resolutions are possible with non-circular, non-rotationally symmetric pupils.

4.3 Multiple lenses for various azimuthal angles

In a previous section we described how arbitrary, azimuthally rotated illumination angles could be achieved with the illuminator. For each angle of interest, a dedicated zoneplate lens is required, designed with its axis rotated to match the central ray direction—each pair of NA and angle-of-incidence values requires one dedicated lens. Mounting the zoneplate array on a rotating stage could also achieve the same objective but would be mechanically complex.

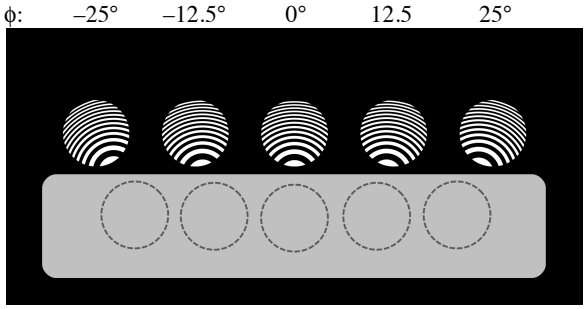

Figure 9. A schematic representation of off-axis zoneplates designed for use at specific azimuthal angles of rotation. The light gray area is a window for the incident beam; black areas are opaque to EUV light. The dashed circles below each zoneplate show the approximate location where the incident beam will pass. The rotation angle of each zoneplate is indicated above.

4.4 Sweet-spot size

The *sweet spot* is defined as the region within the field of view where the quality of the imaging meets given performance metrics. These metrics can include high Strehl ratio, low aberration magnitude, high CD uniformity, and low *x-y* CD measurement difference, for example. While zoneplate lenses can achieve diffraction-limited imaging, their aberrations vary continuously across the field of view, creating a region near the field center where the performance is optimized. For EUV lenses in the AIT and AIT5, this region is a few microns in diameter; and its size is highly dependent on the NA (see Fig. 10). Contrary to our initial assumptions, new analysis indicates that the sweet-spot diameter is not highly sensitive to the focal length of the lens. For a given NA, the sweet spot diameter shrinks with increasing angle of incidence.

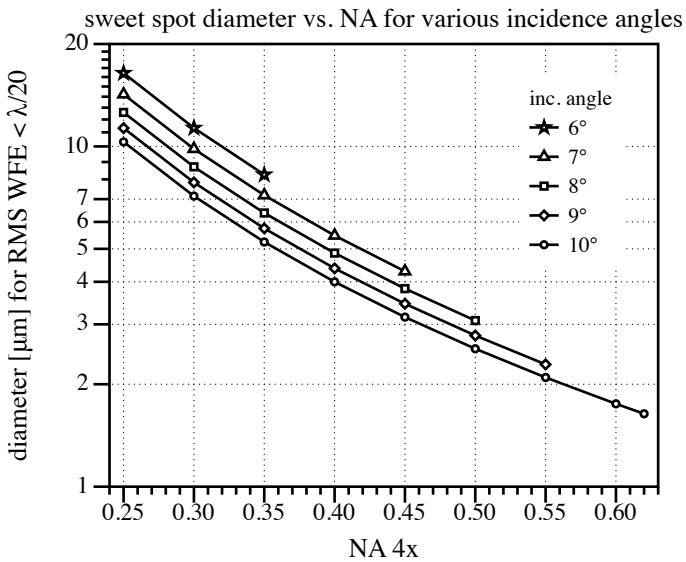

Figure 10. Sweet spot diameter calculated across a range of NA values, for several angles of incidence, based on a λ/20 RMS wavefront error (WFE) metric, excluding defocus. While the sweet spot is nearly circular, within each image, the tilted focal plane limits the vertical dimension to several microns.

Depending on the metrics used, we believe that calculated sweet spot sizes are large enough for line and point-measurements of interest (defects, etc.). Measurements of line properties (critical-dimension, line-width roughness, contrast, normalized image log slope, etc.) are commonly made using 1–2 μm of line length for averaging; such lengths easily fit within the sweet spot based on a λ/20 RMS wavefront error metric. We can anticipate that as lithographically relevant half-pitch values shrink, shorter line lengths will be acceptable for these measurements.

Single-element off-axis lenses have an unavoidable, tilted focal plane in the off-axis direction, giving rise to a field-dependent defocus.[12] The tilt, which increases with the angle of incidence, limits the vertical dimension of the region that can be analyzed within a single image. We believe that it will be possible to synthesize the full sweet spot image from a through-focus image series. However, such a strategy will only be required if large-area imaging is necessary, since the tilt effect is relatively small and has does not significantly compromise data analysis in the AIT.

4.5 Magnification

In the AIT, the typical magnification ratio is 907, but magnification values from 680 to 1000 have been used. With a CCD pixel size of 13.5 μm, this magnification ratio enables an effective pixel size of nearly 15 nm in mask units, significantly oversampling the image relative to the resolution (0.61 λ/NA = 93 nm at 0.0875 NA and 13.4-nm wavelength). In the AIT5 we propose to increase the typical magnification ratio to 1000, giving a nominal pixel size of 13.5 nm.

We can increase the magnification of the imaging system in two ways. Using a constant CCD distance, the magnification can be increased with a shorter zoneplate focal length. Alternately, keeping the zoneplate focal length fixed, we can increase the distance to the CCD camera. In this way we believe magnification ratios from 250 to 4000 will be possible.

4.6 Field of view

As with the AIT, the viewable area of the mask is significantly larger than the aberration-corrected sweet spot of the image. This is extremely important for mask navigation and fine positioning. With a 27.6 mm CCD chip width and a 1000× magnification, the effective mask area viewable at one time is 27.6 μm.

It will be possible, using a dedicated low-magnification zoneplate objective to enable a significantly larger EUV field of view. For example, with 250× magnification (achieved with a long-focal-length, low-NA zoneplate), the viewable field could be expanded to 110 μm.

5. SYSTEM THROUGHPUT

Relative to the AIT, gains in the operational throughput of the AIT5 come from the ease of navigation, focusing and setup at each point, and from a reduction in the exposure time from the more efficient illuminator and zoneplates.

We can predict the AIT5's typical exposure times based on the knowledge of the AIT's current performance and flux level, and by the relative efficiency gain we expect for the new optics. For some elements, the accuracy of these calculations is limited by the unknown reflectivity and contamination levels of the mirrors that will be replaced (or removed). Typical exposure times for most masks in the AIT is 45 s, with approximately 500–1000 photons per pixel when the effective pixel size of 15 nm (mask units). We expect the AIT5 to have exposure times in the range of 1–5 seconds including a 4× increase in the photon density.

The largest efficiency gains come from the following changes. The number of mirrors in the beamline will be reduced by two (one glancing and one 45°), leading to an approximate 2× gain. A gain of 1.25–3× comes from replacing the contaminated Schwarzschild objective with the new illuminator. (The large range comes from the difficulty of predicting both the existing degree of contamination, and the efficiency of the new condenser mirror.) A gain of 2.4× is possible by removing the nitride window in the zoneplate membrane. Other zoneplate improvements are now under investigation.

Including all factors of the design and operation, we anticipate that the AIT5 will be able to record focal series at 5 to 10 locations per hour, depending on the number of images per series.

ACKNOWLEDGMENTS

We wish to acknowledge the support of SEMATECH project leader Hyuk Joo (Harry) Kwon, with great encouragement from David Chan and Bryan Rice, and the SEMATECH Member company leaders who have championed this project. This work was performed under the auspices of the U.S. Department of Energy by the University of California Lawrence Berkeley National Laboratory under management and operating contract DE-AC02-05CH11231. This work was funded by SEMATECH under Agreement No. LB08005006.

REFERENCES

[1] Rice, B., Semiconductor International, June 2009.

[2] Jonckheere, R., EUVL Symposium 2009, oral presentation.

[3] Feldmann, H., Ruoff, J., Harnisch, W., Kaiser W., "Actinic Review of EUV Masks," *Proc. SPIE* **7636**, 76361C (2010).

[4] Hellweg, D., "AIMS™ EUV: the actinic aerial image review platform for EUV masks," *Proc. SPIE* **7969**, *these proceedings*.

[5] Goldberg, K. A., Mochi, I., "Wavelength-Specific Reflections: A Decade of EUV Actinic Mask Inspection Research," *J. Vac. Sci. & Technol. B* **28** (6), C6E1 (2010).

[6] Huh, S., Ren, L., Chan, D., Wurm, S., Goldberg, K., Mochi, I., Nakajima, T., Kishimoto, M., Ahn, B., Kang, I., Park, J., Cho, K., Han, S.-I., Laursen, T., "A study of defects on EUV masks using blank inspection, patterned mask inspection, and wafer inspection," *Proc. SPIE* **7636**, 76360K (2010).

[7] Magana, J. F., Chandhok, M., Crimmins, T. F., Ghadiali, F. A., Liang, T., Zhang, G., "Current status and challenges in EUV reticle defect detection: a case study of using a real product," presented at *SPIE Photomask BACUS*, (2010), *unpublished*.

[8] Huh, S., Rastegar, A., Goodwin, F., Wurm, S., Goldberg, K., Mochi, I., Nakajima, T. Kishimoto, M., Komakine, M., "The Study on the Real Defect on EUV Blankmask and Strategy of EUV Mask Inspection," *Proc. SPIE* **7545**, 75450N (2010).

[9] Kang, I.-Y., Seo, H.-S., Ahn, B.-S., Lee, D.-G., Kim, D., Huh, S., Koh, C.-W., Cha, B., Kim, S.-S., Cho, H.-K., Mochi, I., Goldberg, K. A., "Printability and inspectability study with substrate programmed pit defects at EUV lithography," *Proc. SPIE* **7636**, 76361B (2010).

[10] Naulleau, P., Niakoula, D., Zhang, G., "System-level line-edge roughness limits in extreme ultraviolet lithography," J. Vac. Sci. & Technol. B **26** (6), 1289–93 (2008).

[11] Mochi, I., Goldberg, K. A., Neureuther, A., Xie, R., Yan, P., Yamazoe, K., "Quantitative evaluation of mask phase defects from through-focus EUV aerial images," *Proc. SPIE* **7969**, *these proceedings*.

[12] Goldberg, K. A., Naulleau, P. P., Barty, A., Rekawa, S. B., Kemp, C. D., Gunion, R. F., Salmassi, F., Gullikson, E. M., Anderson, E. H., Han, H.-S., "Performance of actinic EUVL mask imaging using a zoneplate microscope," *Proc. SPIE* **6730**, 67305E (2007).
[13] Goldberg, K. A., Mochi, I., Naulleau, P. P., Han, H.-S., Huh, S., "Benchmarking EUV mask inspection beyond 0.25 NA," *Proc. SPIE* **7122**, 71222E (2008).
[14] Goldberg, K. A., Mochi, I., Huh, S., "Collecting EUV mask images through focus by wavelength tuning," *Proc. SPIE* **7271**, 72713N (2009).
[15] Goldberg, K. A., Barty, A., Liu, Y., Kearney, P., Tezuka, Y., Terasawa, T., Taylor, J. S., Han, H.-S., Wood, O. R. II, "Actinic Inspection of EUV Programmed Multilayer Defects and Cross-Comparison Measurements," J. Vac. Sci. & Technol. B **24** (6), 2824–28 (2006).
[16] Naulleau, P. P., Anderson, C. N., Dean, K., Denham, P., Goldberg, K. A., Hoef, B., LaFontaine, B., Wallow, T., "Recent results from the Berkeley 0.3-NA EUV microfield exposure tool," *Proc. SPIE* **6517**, 65170V (2007).
[17] Chao, W., Kim, J., Rekawa, S., Fischer, P., Anderson, E. H., "Demonstration of 12 nm Resolution Fresnel Zone Plate Lens based Soft X-ray Microscopy," *Opt. Exp.* **17** (20), 17669–77 (2009).
[18] Salmassi, F., Naulleau, P. P., Gullikson, E. M., "Spin-on-glass coatings for the generation of superpolished substrates for use in the extreme-ultraviolet region," *Appl. Opt.* **45** (11), 2404–8 (2006).
[19] Naulleau, P., Goldberg, K., Batson, P., Bokor, J., Denham, P., Rekawa, S., "A Fourier-synthesis custom-coherence illuminator for EUV microfield lithography," *Appl. Opt.* **42** (5), 820–6 (2003).
[20] Naulleau, P., Goldberg, K. A., Batson, P., Denham, P., Rekawa, S., "A synchrotron-based Fourier-synthesis custom-coherence illuminator," *AIP Conf. Proc.* **705**, 792–5 (2004).
[21] Soufli, R., Spiller, E., Schmidt, M., Robbinson, J., Baker, S., Ratti, S., Johnson, M., and Gullikson, E, "Smoothing of diamond-turned substrates for extreme ultraviolet lithography illuminators," *Proc. SPIE* **5193**, 98–104 (2004).
[22] Salmassi, F., Naulleau, P., Gullikson, E., "Spin-on-glass coatings for the generation of superpolished substrates for use in the extreme-ultraviolet region," Appl. Opt. **45** (11), 2404–8 (2006).
[23] Mochi, I., Goldberg, K. A., Naulleau, P., Huh, S., "Improving the performance of the Actinic Inspection Tool with an optimized alignment procedure," *Proc. SPIE* **7271**, 76361A (2009).
[24] A product of KLA-Tencor, http://www.kla-tencor.com/lithography-modeling/chip-prolith.html
[25] Mochi, I., *et al.*, "Aerial image phase measurement: a new dimension in mask metrology," 2010 International Symposium on Extreme Ultraviolet Lithography, October 19, 2010, Kobe, Japan, *oral presentation*.